Research Article | Vol. 7, No. 9 | 1 Sep 2016 | BIOMEDICAL OPTICS EXPRESS 3795
Biomedical Optics EXPRESS

Procedures for risk-stratification of lung cancer using buccal nanocytology

H. SUBRAMANIAN,[1,2,*] P. VISWANATHAN,[1] L. CHERKEZYAN,[1] R. IYENGAR,[2] S. ROZHOK,[2] M. VERLEYE,[2] J. DERBAS,[2] J. CZARNECKI,[1] H. K. ROY,[3] AND V. BACKMAN[1]

[1]*Northwestern University, Biomedical Engineering Department, Evanston, Illinois 60208, USA*
[2]*NanoCytomics LLC, Evanston, Illinois 60201, USA*
[3]*Boston University Medical Center, Boston, Massachusetts, 02118, USA*
[*]*Hariharan@u.northwestern.edu*

Abstract: Lung cancer is the leading cause of cancer deaths in the U.S. with survival dramatically depending on stage at diagnosis. We had earlier reported that nanocytology of buccal cells can accurately risk-stratify smokers for the presence of early and late-stage lung cancer. To translate the technique into clinical practice, standardization of operating procedures is necessary to consistently yield precise and repeatable results. Here, we develop and validate simple, robust, and easily implementable procedures for specimen collection, processing, etc. in addition to a commercially-viable instrument prototype. Results of this work enable translation of the technology from academic lab to physicians' office.

OCIS codes: (110.0180) Microscopy; (110.2960) Image analysis; (120.0120) Instrumentation, measurement, and metrology; (170.1610) Clinical applications.

References and links

1. R. L. Siegel, K. D. Miller, and A. Jemal, "Cancer statistics, 2016," CA Cancer J. Clin. **66**(1), 7–30 (2016).
2. P. B. Bach, G. A. Silvestri, M. Hanger, and J. R. Jett, "Screening for lung cancer: ACCP evidence-based clinical practice guidelines (2nd edition)," Chest **132**, 69S–77S (2007).
3. T. Neumann, M. Meyer, F. W. Patten, F. L. Johnson, Y. S. Erozan, W. J. Frable, P. K. Gupta, M. B. Zaman, and A. C. Nelson, "Premalignant and Malignant Cells in Sputum from Lung Cancer Patients," Cancer **117**(6), 473–481 (2009).
4. T. C. Kennedy, S. P. Proudfoot, W. A. Franklin, T. A. Merrick, G. Saccomanno, M. E. Corkill, D. L. Mumma, K. E. Sirgi, Y. E. Miller, P. G. Archer, and A. Prochazka, "Cytopathological analysis of sputum in patients with airflow obstruction and significant smoking histories," Cancer Res. **56**(20), 4673–4678 (1996).
5. E. K. J. Risse, G. P. Vooijs, and M. A. van't Hof, "Diagnostic Significance of "Severe Dysplasia" in Sputum Cytology," Acta Cytol. **32**(5), 629–634 (1988).
6. Y. P. Sher, J. Y. Shih, P. C. Yang, S. R. Roffler, Y. W. Chu, C. W. Wu, C. L. Yu, and K. Peck, "Prognosis of non-small cell lung cancer patients by detecting circulating cancer cells in the peripheral blood with multiple marker genes," Clin. Cancer Res. **11**(1), 173–179 (2005).
7. C. Wu, H. Hao, L. Li, X. Zhou, Z. Guo, L. Zhang, X. Zhang, W. Zhong, H. Guo, R. M. Bremner, and P. Lin, "Preliminary investigation of the clinical significance of detecting circulating tumor cells enriched from lung cancer patients," J. Thorac. Oncol. **4**(1), 30–36 (2009).
8. S. S. Devesa, F. Bray, A. P. Vizcaino, and D. M. Parkin, "International lung cancer trends by histologic type: male:female differences diminishing and adenocarcinoma rates rising," Int. J. Cancer **117**(2), 294–299 (2005).
9. H. Welch, S. Woloshin, L. Schwartz, L. Gordis, P. Gotzsche, R. Harris, B. Kramer, and D. Ransohoff, "Overstating the Evidence for Lung Cancer Screening: The I-ELCAP Study and its News Coverage," Arch. Intern. Med. **167**(21), 2289 (2007).
10. D. A. Lieberman, J. Holub, G. Eisen, D. Kraemer, and C. D. Morris, "Utilization of colonoscopy in the United States: results from a national consortium," Gastrointest. Endosc. **62**(6), 875–883 (2005).
11. J. M. Croswell, S. G. Baker, P. M. Marcus, J. D. Clapp, and B. S. Kramer, "Cumulative incidence of false-positive test results in lung cancer screening: a randomized trial," Ann. Intern. Med. **152**, 505–512 (2010).
12. T. R. Church, W. C. Black, D. R. Aberle, C. D. Berg, K. L. Clingan, F. Duan, R. M. Fagerstrom, I. F. Gareen, D. S. Gierada, G. C. Jones, I. Mahon, P. M. Marcus, J. D. Sicks, A. Jain, and S. Baum; National Lung Screening Trial Research Team, "Results of initial low-dose computed tomographic screening for lung cancer," N. Engl. J. Med. **368**(21), 1980–1991 (2013).
13. L. L. Humphrey, M. Deffebach, M. Pappas, C. Baumann, K. Artis, J. P. Mitchell, B. Zakher, R. Fu, and C. G. Slatore, "Screening for lung cancer with low-dose computed tomography: a systematic review to update the US Preventive services task force recommendation," Ann. Intern. Med. **159**(6), 411–420 (2013).

#268778 http://dx.doi.org/10.1364/BOE.7.003795
Journal © 2016 Received 20 Jun 2016; revised 13 Aug 2016; accepted 20 Aug 2016; published 31 Aug 2016

Biomedical Optics EXPRESS

14. K. Steiling, J. Ryan, J. S. Brody, and A. Spira, "The field of tissue injury in the lung and airway," Cancer Prev. Res. (Phila.) **1**(6), 396–403 (2008).
15. G. D. Dakubo, J. P. Jakupciak, M. A. Birch-Machin, and R. L. Parr, "Clinical implications and utility of field cancerization," Cancer Cell Int. **7**(1), 2 (2007).
16. B. J. Braakhuis, M. P. Tabor, J. A. Kummer, C. R. Leemans, and R. H. Brakenhoff, "A genetic explanation of Slaughter's concept of field cancerization: evidence and clinical implications," Cancer Res. **63**(8), 1727–1730 (2003).
17. A. Spira, J. Beane, V. Shah, G. Liu, F. Schembri, X. Yang, J. Palma, and J. S. Brody, "Effects of cigarette smoke on the human airway epithelial cell transcriptome," Proc. Natl. Acad. Sci. U.S.A. **101**(27), 10143–10148 (2004).
18. A. Spira, J. E. Beane, V. Shah, K. Steiling, G. Liu, F. Schembri, S. Gilman, Y. M. Dumas, P. Calner, P. Sebastiani, S. Sridhar, J. Beamis, C. Lamb, T. Anderson, N. Gerry, J. Keane, M. E. Lenburg, and J. S. Brody, "Airway epithelial gene expression in the diagnostic evaluation of smokers with suspect lung cancer," Nat. Med. **13**(3), 361–366 (2007).
19. L. Kopelovich, D. E. Henson, A. F. Gazdar, B. Dunn, S. Srivastava, G. J. Kelloff, and P. Greenwald, "Surrogate anatomic/functional sites for evaluating cancer risk: an extension of the field effect," Clin. Cancer Res. **5**(12), 3899–3905 (1999).
20. D. Sidransky, "The Oral Cavity as a Molecular Mirror of Lung Carcinogenesis," Cancer Prev. Res. (Phila.) **1**(1), 12–14 (2008).
21. J. O. Boyle, Z. H. Gümüs, A. Kacker, V. L. Choksi, J. M. Bocker, X. K. Zhou, R. K. Yantiss, D. B. Hughes, B. Du, B. L. Judson, K. Subbaramaiah, and A. J. Dannenberg, "Effects of cigarette smoke on the human oral mucosal transcriptome," Cancer Prev. Res. (Phila.) **3**(3), 266–278 (2010).
22. M. Bhutani, A. K. Pathak, Y.-H. Fan, D. D. Liu, J. J. Lee, H. Tang, J. M. Kurie, R. C. Morice, E. S. Kim, W. K. Hong, and L. Mao, "Oral Epithelium as a Surrogate Tissue for Assessing Smoking-Induced Molecular Alterations in the Lungs," Cancer Prev. Res. (Phila.) **1**(1), 39–44 (2008).
23. T. Shani, A. Onn, A. Kabha, I. Ben-Dov, I. Adam, N. Amariglio, R. Yahalom, G. Rechavi, L. Trakhtenbrot, and A. Hirshberg, "Chromosomal numerical aberrations in apparently normal oral mucosa of heavy smokers affected by lung cancer," Oral Oncol. **46**(2), 96–99 (2010).
24. J. Sanz-Ortega, F. Roig, M. M. Al-Mousa, M. C. Saez, A. Muñoz, J. Sanz-Esponera, and L. Callol, "17p13 (p53 locus), 5q21 (APC locus) and 9p21 (p16 locus) allelic deletions are frequently found in oral exfoliative cytology cells from smoker patients with non-small-cell lung cancer," Histol. Histopathol. **22**(5), 541–545 (2007).
25. M. Us-Krasovec, J. Erzen, M. Zganec, M. Strojan-Flezar, J. Lavrencak, D. Garner, A. Doudkine, and B. Palcic, "Malignancy associated changes in epithelial cells of buccal mucosa: a potential cancer detection test," Anal. Quant. Cytol. Histol. **27**(5), 254–262 (2005).
26. R. A. Kemp and B. Turic, "Can early lung cancer be detected from buccal mucosal scrapings?" Chest **128**(4), 154S (2005).
27. H. Subramanian, P. Pradhan, Y. Liu, I. R. Capoglu, X. Li, J. D. Rogers, A. Heifetz, D. Kunte, H. K. Roy, A. Taflove, and V. Backman, "Optical methodology for detecting histologically unapparent nanoscale consequences of genetic alterations in biological cells," Proc. Natl. Acad. Sci. U.S.A. **105**(51), 20118–20123 (2008).
28. H. K. Roy, C. B. Brendler, H. Subramanian, D. Zhang, C. Maneval, J. Chandler, L. Bowen, K. L. Kaul, B. T. Helfand, C. H. Wang, M. Quinn, J. Petkewicz, M. Paterakos, and V. Backman, "Nanocytological field carcinogenesis detection to mitigate overdiagnosis of prostate cancer: a proof of concept study," PLoS One **10**(2), e0115999 (2015).
29. L. Cherkezyan, Y. Stypula-Cyrus, H. Subramanian, C. White, M. Dela Cruz, R. K. Wali, M. J. Goldberg, L. K. Bianchi, H. K. Roy, and V. Backman, "Nanoscale changes in chromatin organization represent the initial steps of tumorigenesis: a transmission electron microscopy study," BMC Cancer **14**(1), 189 (2014).
30. V. J. Konda, L. Cherkezyan, H. Subramanian, K. Wroblewski, D. Damania, V. Becker, M. H. Gonzalez, A. Koons, M. Goldberg, M. K. Ferguson, I. Waxman, H. K. Roy, and V. Backman, "Nanoscale markers of esophageal field carcinogenesis: potential implications for esophageal cancer screening," Endoscopy **45**(12), 983–988 (2013).
31. H. K. Roy, D. P. Damania, M. DelaCruz, D. P. Kunte, H. Subramanian, S. E. Crawford, A. K. Tiwari, R. K. Wali, and V. Backman, "Nano-architectural alterations in mucus layer fecal colonocytes in field carcinogenesis: potential for screening," Cancer Prev. Res. (Phila.) **6**(10), 1111–1119 (2013).
32. Y. Stypula-Cyrus, D. Damania, D. P. Kunte, M. D. Cruz, H. Subramanian, H. K. Roy, and V. Backman, "HDAC up-regulation in early colon field carcinogenesis is involved in cell tumorigenicity through regulation of chromatin structure," PLoS One **8**(5), e64600 (2013).
33. D. Damania, H. K. Roy, D. Kunte, J. A. Hurteau, H. Subramanian, L. Cherkezyan, N. Krosnjar, M. Shah, and V. Backman, "Insights into the field carcinogenesis of ovarian cancer based on the nanocytology of endocervical and endometrial epithelial cells," Int. J. Cancer **133**(5), 1143–1152 (2013).
34. D. Damania, H. K. Roy, H. Subramanian, D. S. Weinberg, D. K. Rex, M. J. Goldberg, J. Muldoon, L. Cherkezyan, Y. Zhu, L. K. Bianchi, D. Shah, P. Pradhan, M. Borkar, H. Lynch, and V. Backman, "Nanocytology of rectal colonocytes to assess risk of colon cancer based on field cancerization," Cancer Res. **72**(11), 2720–2727 (2012).
35. H. Subramanian, H. K. Roy, P. Pradhan, M. J. Goldberg, J. Muldoon, R. E. Brand, C. Sturgis, T. Hensing, D. Ray, A. Bogojevic, J. Mohammed, J. S. Chang, and V. Backman, "Nanoscale cellular changes in field carcinogenesis detected by partial wave spectroscopy," Cancer Res. **69**(13), 5357–5363 (2009).

Biomedical Optics EXPRESS

36. D. Damania, H. Subramanian, A. K. Tiwari, Y. Stypula, D. Kunte, P. Pradhan, H. K. Roy, and V. Backman, "Role of Cytoskeleton in Controlling the Disorder Strength of Cellular Nanoscale Architecture," Biophys. J. **99**(3), 989–996 (2010).
37. L. Cherkezyan, I. Capoglu, H. Subramanian, J. D. Rogers, D. Damania, A. Taflove, and V. Backman, "Interferometric Spectroscopy of Scattered Light Can Quantify the Statistics of Subdiffractional Refractive-Index Fluctuations," Phys. Rev. Lett. **111**(3), 033903 (2013).
38. N. N. Boustany, S. A. Boppart, and V. Backman, "Microscopic Imaging and Spectroscopy with Scattered Light," Annu. Rev. Biomed. Eng. **12**(1), 285–314 (2010).
39. O. Graydon, N. Horiuchi, D. Pile, S. Pleasants, and R. Won, "Comex Media: Subtle Sensing," Nat. Photonics **7**(10), 763 (2013).
40. V. Konda, L. Cherkezyan, H. Subramanian, K. Wroblewski, D. Damania, V. Becker, M. Goldberg, J. Chennat, L. Karl, M. Ferguson, I. Waxman, H. Roy, and V. Backman, "Nanoscale markers of esophageal field carcinogenesis: potential implications for esophageal cancer screening," Endoscopy **45**, 983–988 (2013).
41. X. Meng, Y. Zhang, L. Lao, R. Saito, A. Li, C. M. Bäckman, B. M. Berman, K. Ren, P. K. Wei, and R. X. Zhang, "Spinal interleukin-17 promotes thermal hyperalgesia and NMDA NR1 phosphorylation in an inflammatory pain rat model," Pain **154**(2), 294–305 (2013).
42. H. K. Roy, T. Hensing, and V. Backman, "Nanocytology for field carcinogenesis detection: novel paradigm for lung cancer risk stratification," Future Oncol. **7**(1), 1–3 (2011).
43. A. K. Tiwari, H. Subramanian, C. D. Maneval, R. K. Wali, V. Backman, and H. K. Roy, "Partial wave spectroscopic microscopy: a novel tool to assess perturbation in the cellular transcriptional activity during colon carcinogenesis," Gastroenterology **144**(5), S175 (2013).
44. H. G. Davies, M. H. F. Wilkins, J. Chayen, and L. F. La Cour, "The use of interference microscope to determine dry mass in living cells and as a quantitative cytochemical method," Q. J. Microsc. Sci. **95**, 271–304 (1954).
45. L. Cherkezyan, H. Subramanian, and V. Backman, "What structural length scales can be detected by the spectral variance of a microscope image?" Opt. Lett. **39**(15), 4290–4293 (2014).
46. B. Deng, S. Melnik, and P. R. Cook, "Transcription factories, chromatin loops, and the dysregulation of gene expression in malignancy," Semin. Cancer Biol. **23**(2), 65–71 (2013).
47. K. Kumar, A. K. Abbas, J. C. Aster, and N. Fausto, *Robbins & Cotran Pathologic Basis of Disease*, 8th ed., Robbins Pathology (Saunders, 2009).
48. J. E. Chandler, H. Subramanian, C. D. Maneval, C. A. White, R. M. Levenson, and V. Backman, "High-speed spectral nanocytology for early cancer screening," J. Biomed. Opt. **18**(11), 117002 (2013).
49. D. Zhang, L. Cherkezyan, I. Capoglu, H. Subramanian, J. Chandler, S. Thompson, A. Taflove, and V. Backman, "Spectroscopic microscopy can quantify the statistics of subdiffractional refractive-index fluctuations in media with random rough surfaces," Opt. Lett. **40**(21), 4931–4934 (2015).
50. L. Cherkezyan, H. Subramanian, V. Stoyneva, J. D. Rogers, S. Yang, D. Damania, A. Taflove, and V. Backman, "Targeted alteration of real and imaginary refractive index of biological cells by histological staining," Opt. Lett. **37**(10), 1601–1603 (2012).
51. E. S. Cibas and B. S. Ducatman, *Cytology: Diagnostic Principles and Clinical Correlates* (W.B. Saunders, Philadelphia, 1996), pp. xiv, 371.
52. H. K. Roy, H. Subramanian, D. Damania, T. A. Hensing, W. N. Rom, H. I. Pass, D. Ray, J. D. Rogers, A. Bogojevic, M. Shah, T. Kuzniar, P. Pradhan, and V. Backman, "Optical Detection of Buccal Epithelial Nanoarchitectural Alterations in Patients Harboring Lung Cancer: Implications for Screening," Cancer Res. **70**(20), 7748–7754 (2010).

1. Introduction

With an estimated 224,390 new cases in 2016, Lung Cancer is the leading cause of cancer deaths among Americans resulting in over 158,080 new deaths in 2016 [1]. Five year survival rates (~15%) are dictated by the stage at diagnosis (stage 1 ~90%, stage 4 ~2%). Only 16% of cancers are diagnosed at a localized stage (stage 1) since most patients only seek medical attention for symptoms that are harbingers of an advanced, incurable disease. Smoking is the most prevalent risk factor, which accounts for ~90% of lung cancers in men and ~80% in women. If diagnosed early, patients with lung cancer have good survival rates. Lung cancer is an ideal malignancy for screening because the at-risk population (current/former smokers) is well defined.

Standard approaches for lung cancer screening currently lack sensitivity [2]. In particular, the sensitivity of sputum cytology is affected by the difficulty of specimen collection (only induced sputum based methods), the low number of diagnostic cells in sputum (akin to finding a needle in a haystack), and the experience of a cytologist [3–5]. The use of circulating tumor cells (CTCs) for screening has similar drawbacks, including the low yield of CTCs in early stages of cancer, the purity of CTCs, and the complex isolation procedures [6, 7]. Bronchoscopy has potential for identifying early tumors in the central airways via

Biomedical Optics EXPRESS

autofluorescence. However, bronchoscopy is invasive, expensive, and insensitive to peripheral lesions [8]. Recently, low-dose CT (LDCT) for lung cancer has gained significant interest, and in a recent study of ~50,000 patients, LDCT led to a 20% drop in deaths from lung cancer [9–12]. This spurred the USPSTF to recommend using LDCT for screening for lung cancer in high-risk patients [13]. However, false positives are the major challenge in the clinical implementation of LDCT; the incidental finding is associated with anxiety, cost and complications of unnecessary procedures. Moreover, with a lung cancer prevalence rate of ~1% in smokers, it is impractical to screen the entire at-risk population using LDCT. Thus a simple, accurate and minimally-intrusive tool that can be performed in a primary care physician's (PCP) office to risk stratify patients for further LDCT screening is urgently needed.

Our approach to lung cancer risk-stratification is based on the detection of lung field carcinogenesis. In its simplest form, field carcinogenesis is the concept that the genetic/environmental milieu that results in a neoplastic lesion in one area of the organ is diffusely present either in the organ itself or neighboring organs that share the same "field of injury" [14]. That is, a fertile environment of abnormal genetic modifications is primed for individual tumor and lesion growth. Therefore, the cells in the neoplastic field can be used to identify and study the earliest events in cancer progression [15, 16]. Lung cancer epitomizes the field carcinogenesis. The entire aero-digestive mucosa is "condemned" by tobacco exposure, leaving patients with lung cancer at risk for synchronous or metachronous new neoplastic lesions in the lungs. One pathway for lung carcinogenesis is the alteration, from smoking, of gene expression throughout the microscopically normal bronchial epithelium [17]. For example, the potential screening applications have been underscored by a landmark report by Spira et al. [18] on the microarray analysis from visually normal right mainstem bronchial epithelium from smokers with and without concurrent lung cancer [18]. While the bronchial epithelium clearly shows promise for identifying lung field carcinogenesis, it is far too intrusive for screening. From an accessibility and practicality point of view, the oral and nasal epithelia are more attractive candidate sites. The oral and nasal epithelia are exposed to the same field of injury (i.e., tobacco smoke) as the bronchial epithelium and are encompassed in lung field carcinogenesis [19]. Indeed, Sidransky has espoused a concept that the oral cavity is a "molecular mirror" of the bronchial epithelium [20] with several evidences supporting this concept [18, 21–25]. While there are numerous reports on the buccal mucosa as a marker for lung cancer, only a handful of reports focus on its diagnostic performance [26]. Thus, there is a strong proof of principle that buccal interrogation can be used to predict lung cancer, despite the inadequacy of current markers for clinical use.

This manuscript is based on a novel cancer risk-stratification technique, Partial Wave Spectroscopic (PWS) nanocytology, which quantifies the statistical properties of intracellular nanoarchitecture. Using this PWS nanocytology technique, our group has demonstrated that an increase in the 'disorder of cell nanoarchitecture' is one of the earliest events in carcinogenesis, preceding any known microscale and molecular alterations [27–36]. Importantly, this is a property of early-stage tumor cells as well as a marker of field carcinogenesis [30, 33–36]. Our goal was to develop a new cancer risk stratification paradigm where the presence of a cancerous tumor is detected by a simple swab of histologically normal cells from an easily accessible surrogate site via PWS identification of field carcinogenesis. Data from more than 1000 patients in multiple cancer types (colon, lung, pancreas, esophagus, ovarian etc.) shows that PWS analysis of cells from surrogate sites could discriminate between cancer-free and cancer-harboring patients. For example, the presence of risk for lung cancer can be detected by a simple buccal swab of histologically normal buccal (cheeks) cells. Our preliminary data from 135 patients showed that buccal PWS analysis could discriminate between cancer-free smokers vs. lung cancer patients with a single PWS marker [36].

Biomedical Optics EXPRESS

As discussed above, buccal PWS shows promise to be a low-cost, highly-sensitive, minimally-invasive, population-wide risk stratification test for lung cancer. However, a number of steps are needed to translate the technology from the academic setting into clinical practice. In this manuscript, we report a simple, easy to use, standardized protocol for buccal PWS that was developed using 653 human buccal specimens from clinical patients and healthy volunteers. Similarly, we report developing a commercialization ready PWS nanocytology prototype that can acquire a patient specimen in a clinically acceptable time of ~30 minutes. We have validated both our instrument and the standardized protocol in a clinical study performed on 37 human subjects containing 11 smokers with no cancer present and 26 smokers with lung cancer. Our results indicate that the new standardized protocol reduces the user variability and inter-patient/intra-patient variability and has the diagnostic performance that is comparable to those reported in the preliminary results. The next step will be to perform a multi-center clinical validation trial that would form the basis for the eventual regulatory approval.

2. Methods

2.1 PWS nanocytology: a new technique to study cell nanostructure

The resolution of conventional microscopic histopathology is limited to ~200 nm. In order to assess the nanoscale alterations due to field carcinogenesis, PWS nanocytology couples spectroscopy with microscopy [27]. The principles of PWS nanocytology are discussed in multiple publications [27, 33–43], and here we provide only a brief summary. The technique is grounded in the finding that while sub-diffractional length scales are not resolvable, they are still detectable through the analysis of elastically scattered light. At a given location within a cell, the refractive index (RI) n is proportional to the local density (ρ) of macromolecules (proteins, DNA, RNA) with the refraction increment nearly independent of the chemical composition [44]. Therefore, the spatial variations of macromolecular density can be measured once the fluctuations of RI are known.

The goal of PWS nanocytology is to measure the nanoscale structure within biological cells which cannot be otherwise imaged using conventional optics-based techniques. Hence, a high sensitivity to subdiffractional RI variations and a minimal sensitivity to larger length scales are both required. To achieve this objective, PWS nanocytology performs spectral analysis on images recorded from a reflected-light bright-field microscope with a spectrally-resolved image acquisition, a small-to-moderate numerical aperture (NA) of light incidence, and a large NA of light collection. In the vertical direction, RI of the sample is matched on one side and mismatched at the other, which is achieved by depositing fixed biological cells on glass microscopy slides and exposing their top surface to air. The wavelength-dependent signal registered by each pixel of the microscope image represents the optical interference between a reference wave and the light scattered from all RI variations within an intracellular volume defined by the spatial coherence in the transverse plane and the cell thickness longitudinally. The second order statistic Σ^2 of the recorded interference spectra is used to measure the statistics of the spatial variations of intracellular macromolecular density using equations in Ref [37]. with sensitivity to RI correlation length L_C ~20 - 200 nm [45]. For small L_C, Σ is proportional to the characteristic lengthscale of macromolecular arrangement L_C and the standard deviation of RI fluctuations δ_n. For large L_C, Σ becomes independent of the sample's characteristic lengthscale. Therefore, the signal registered from small L_C is not weighed down by that obtained from large L_C. Moreover, the structural changes at length scales >200nm, which are naturally resolved in the microscope image, do not affect Σ [37].

Once the spectrally-resolved image is acquired, Σ is calculated for each pixel yielding the $\Sigma(x,y)$ spatially-resolved map quantifying the macromolecular density distribution inside the cell. A higher Σ implies a more heterogeneous density distribution: both L_C and δ_n increase. For example, when PWS is used to image the cell nucleus, Σ probes higher order chromatin structure which is intimately related to global gene transcription underscoring its importance

Biomedical Optics EXPRESS

in cancer biology [41, 43]. Nanoscale morphology of the chromatin with a higher Σ appears rough and clumped [29]. Similar alterations at larger, micron scales ("rough chromatin") are a widely used histological marker of dysplasia and malignancy [46, 47].

2.2 High-throughput PWS (HT-PWS) instrument

The HT-PWS nanocytology instrument is discussed in detail in [48], while here we provide a brief summary. HT-PWS is a reflected-light bright-field microscope with spectrally-resolved image acquisition, a moderate NA of light incidence (NA = 0.3), and a large NA of light collection (NA = 0.6). The HT-PWS instrument uses Köhler illumination scheme for the uniformity of illumination light intensity across the field of view and a high-speed acousto-optical tunable filter (AOTF, Orlando, Florida) to selectively filter the wavelength of the illuminating light from 450 to 700nm (step size 1nm, filter bandwidth 3nm) and achieve wavelength-resolved image acquisition. As a result, three-dimensional data cubes (x, y, λ) are saved representing the raw data from every measurement [48].

To maximize the speed of PWS data acquisition and minimize user-intensive work, high-speed automated hardware controlled via custom-written software (Matlab, Mathworks, Inc.) was implemented [48]. The automated hardware includes: (i) two linear sample stages (Zaber Technologies) for scanning the sample in the transverse plane, (ii) one linear stage (Zaber Technologies) for moving the sample stage longitudinally and automatically focusing the image, and (iii) one objective turret for switching between low-magnification (10X, UPlanFL N, Olympus) mapping of full specimen slides and high-magnification (40X) imaging of PWS data acquisition. The custom-developed software includes (i) automated low-magnification slide-mapping for the user to interactively choose the cells suitable for the study followed by (ii) automated collection of PWS data from the selected cells, (iii) automated microscope focusing before any data acquisition, and (iv) automatic registration of transmission images of all cells used in the study using the transmission arm. A brief discussion of the translation from the HT-PWS system to the commercial-ready PWS system is made in the *Results and Discussion* section. Figure 1(a) shows the schematic of the HT-PWS instrument and the optical path while Fig. 1(b) shows the work flow of the buccal PWS nanocytology using the HT-PWS system.

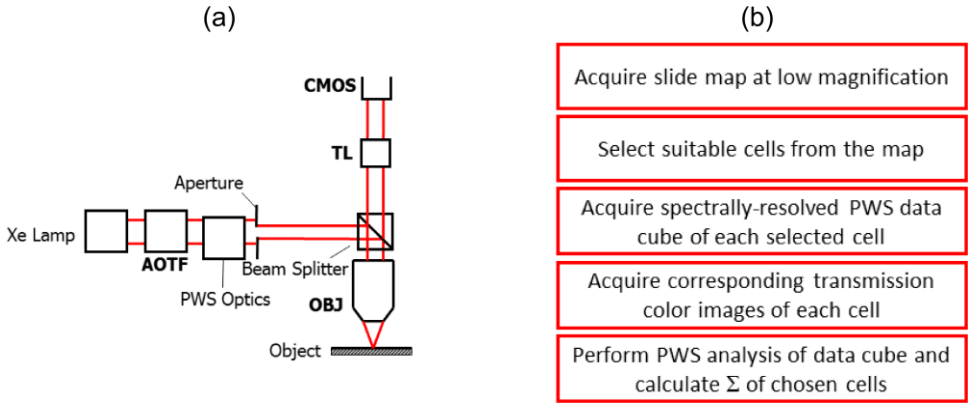

Fig. 1. (a) Schematic of the Partial Wave Spectroscopic (PWS)Microscopy instrument. White light is incident from a Xenon (Xe) lamp using Kohler illumination microscope light path (PWS Optics)| through the objective (OBJ) onto the sample. Spectrally-resolved microscope image is registered on a charge coupled device (CCD)| camera using a spectral filter (SF, either a slit spectrometer or a liquid-crystal tunable filter). TL denotes atube lens. (b) Measurement work flow of the buccal partial wave spectroscopic (PWS) nanocytology.

Biomedical Optics EXPRESS

2.3 Data analysis

Data analysis was performed using Matlab (MathWorks, Inc.) computing software. Raw PWS nanocytology data is a three-dimensional matrix (x, y, λ), comprised of reflectance spectra for every pixel (x, y), recorded at wavelengths from 450 to 700nm with 1nm step size. The raw spectra were processed using a low-pass butterworth filter of 6th order with a frequency cutoff 0.2. To calculate two-dimensional maps $\Sigma(x,y)$ for each measurement, a second-order polynomial was fitted to and subtracted from each spectrum, eliminating the effects of surface roughness [49], followed by a standard deviation calculation to yield $\Sigma(x,y)$. Finally, a region of interest consisting of the central 50% of cellular area was selected using a custom-written automated software and the mean Σ across pixels within the selected area was calculated. The patient mean Σ was calculated as the average Σ of all measured cells after outlier removal was performed (Outliers were defined as Σ values that were either above Q3 + 1.5*IQR, or below Q1-1.5*IQR, where Q1 and Q3 are first and third quartiles respectively and IQR is the interquartile range of data distribution for the particular patient.)

2.4 Statistical analysis

The *number of cells* per specimen needed to acquire for the Confidence Interval on mean Σ (defined in 2.3) to be <5% of the difference between lung cancer and control subjects is ~30. The other statistical analyses were performed as follows: intra-patient variability was defined as the standard deviation of the 30 Σ values calculated from different cells measured from the same patient relative to their across-cell mean value. In turn, inter-patient variability was defined as the standard deviation of mean Σ values calculated from different patients within the same diagnostic category relative to their across-patient mean value. P-values were calculated using an in-built function ttest2, performing Student's unpaired t-test assuming unequal variances of the two data sets. Effect size (ES) was calculated as the difference between the means of two groups in the units of the cumulative standard deviation, defined as the square root of the sum of variances of the two groups. As an example, an Effect size > 80% is considered to be very good when comparing the differences between two groups while the Effect size < 30% is considered to be poor. In the entire manuscript, Effect size is considered a major statistical parameter to compare the diagnostic difference between patients with and without lung cancer. Correlation between two predictors per one observation (here, Σ of superficial and Σ of intermediate cells) was evaluated using Pearson Product-Moment Correlation Coefficient for the two sets of values. For the multivariate analysis, a linear regression model was used to combine the two predictors per observation, after which an in-built function perfcurve was used to generate the receiver operating characteristic (ROC) curve that illustrates the true positive and the false positive rates at various diagnostic threshold settings, calculate the area under the curve (AUC), and determine the sensitivity and specificity of the diagnostic test based the optimal threshold value.

2.5 Clinical recruitment and protocol

The patient categories in this study included: healthy volunteers, smokers with no lung cancers and smokers with lung cancer. The lung cancer patients were selected across different stages (Stage I-IV) and across different histologies of cancer (non-small cell lung cancer, small cell lung cancer, adenocarcinoma etc). Lung cancer patients were recruited based on confirmed histological diagnosis post-surgery but prior to any therapy.

The protocol defined for the preliminary academic study to process all clinical subject samples followed: (a) Collection – samples were collected at the clinical site using a Cytobrush (Coopersurgical, CT), (b) Deposition – samples were deposited on a glass slide at the clinical site using a smear technique, (c) Fixation – samples were fixed on the slide at the clinical site in 95% ethanol, (d) Transport – temperature controls were not applied when samples were transported, (e) Storage – samples were stored at 4°C until they were stained

Biomedical Optics EXPRESS

and data was acquired, (f) Staining – samples were stained (conventional Haematoxylin and Cytostain) in the lab without any significant restrictions on time of staining from the time of fixation.

After extensive conversations with physicians and clinical coordinators, it was understood that the sample collection and processing protocol that was used in the preliminary academic study had limitations for successful translation into clinical practice. These limitations include: (a) user variability of smearing cells onto the glass slide (e.g., variability in brushing pressure, number of rotations etc.), (b) extensive cell transfer and sample fixation processes at the physician office, and (c) inadequate control over transport and storage conditions. These limitations are addressed by developing a more robust and easy to implement protocol which is discussed in detail in sections 3.1 to 3.3.

3. Results and discussion

In order to successfully translate the buccal PWS nanocytology into clinical practice, we first developed a simple and robust process workflow (Fig. 2). The first step in the process involves shipment of a collection kit, consisting of critical cell collection and storage components, to clinical sites for collection of a patient specimen. After the PCP prescribes the lung test, the nurse/clinical coordinator will collect the sample and ship them to the centralized lab. In the centralized lab, the samples will be processed and analyzed, after which the test report will be electronically sent to the PCP office. Once the test results are received, the PCP will review the results and suggest the next step for the patients.

In order to implement this process flow and develop a standard operating procedure, our group improved the individual steps involved in the protocol discussed in Section 2.5. This involves (i) designing a robust cell collection and deposition technique to reduce the variability due to traditional manual deposition process, (ii) determining the optimal storage and transport conditions such as the storage temperature, time of storage of the patient specimens, etc., (iii) developing optimal fixation and staining to optimize the sample processing conditions, (iv) defining a robust cell selection criteria to reduce the variability of the PWS measurements and to improve the overall diagnostic performance.

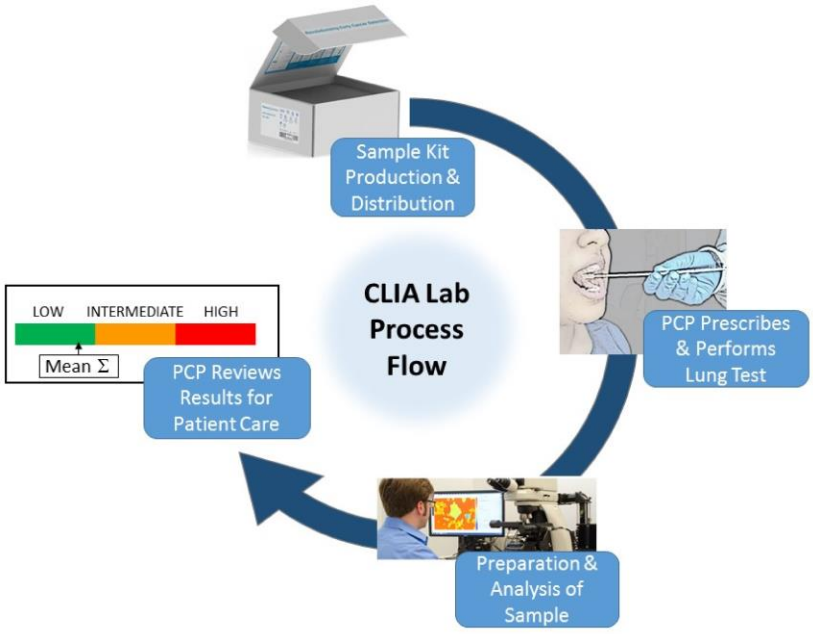

Fig. 2. Work flow of the buccal partial wave spectroscopic (PWS) nanocytology process that will enable clinical translation of the technology.

Biomedical Optics EXPRESS

3.1 Optimal characteristics for a good quality specimen slide

Development of standard operating procedures requires identification of specimen characteristics that contribute to the diagnostic performance. To identify these characteristics, samples were obtained from 49 clinical patients (smokers without lung cancer = 32; smokers with lung cancer = 17) following the protocol discussed in Section 2.5. In this study 150-200 cells were acquired from each patient specimen slide. The cells were further classified into the following categories based on its characteristics: (i) Non-overlapping, unfolded, isolated cells, (ii) Overlapping and folded cells, (iii) Cells with a visible and prominent nuclei, and (iv) Cells with no nuclei present. Figure 3 illustrates examples of cells that are overlapping (Fig. 3(a)), folded within itself (Fig. 3(b)), and non-overlapping (Fig. 3(c)) with the corresponding Σ images (Fig. 3(d)-3(f)). The patient specimen slides that had < 20 cells in any of these categories were removed from the final diagnosis. The results indicated that the non-overlapping and non-folded cells with a prominent, centrally-located nucleus have a much better diagnostic performance (Effect size = 96%; Sensitivity = 89%; Specificity = 90%) than the cells that are folded, overlapping, or with no nuclei present (Effect size = 38%; Sensitivity = 67%; Specificity = 75%). Importantly, the folded cells had a much higher intercellular variability of Σ (> 40%) compared to the unfolded cells (~25%).

These observations were further validated in two independent studies. The first study comprising 17 patients (12 smokers without lung cancer; 5 smokers with lung cancer) yielded poor diagnosis (ES < 30%) due to folded and overlapping cells chosen for analysis. In the second study comprising 73 patients (41 control patients without lung cancer; 32 patients with lung cancer), choosing non-overlapping and non-folded isolated cells yielded a high diagnostic performance (ES ~90%).

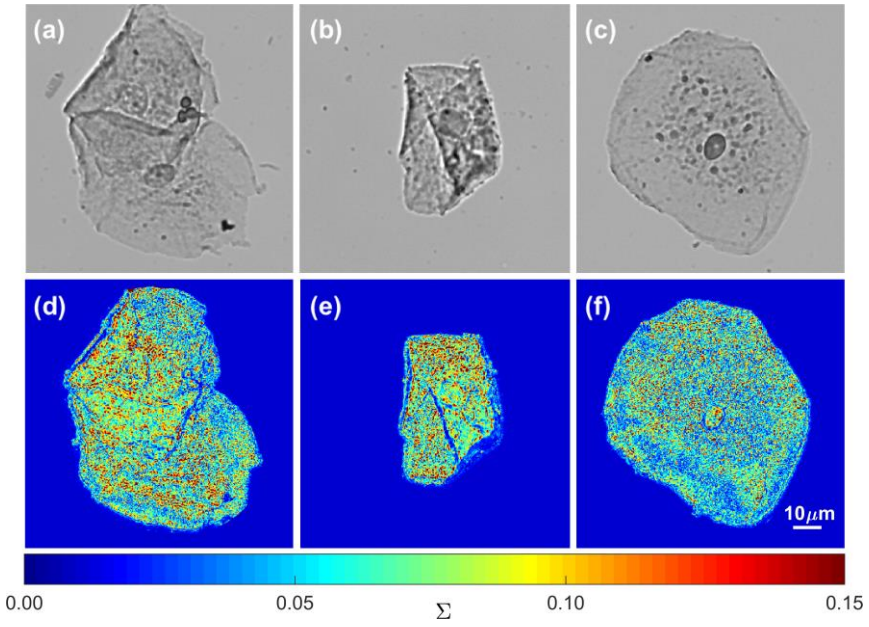

Fig. 3. Examples of buccal squamous epithelial cells found on prepared specimen slides. (a) Representative transmission image of two overlapping cells and (d) the corresponding spatially resolved map Σ(*x, y*) calculated by PWS. (b) Example of a folded isolated cell and (e) the corresponding map of Σ. (c) Isolated, non-folded cell classified as "suitable" for our study and (f) the corresponding Σ(*x, y*).

From the results of these 139 human clinical specimens, we developed the following optimal characteristics of good quality specimen slides: (a) > 70% of cells present in a slide

Biomedical Optics EXPRESS

form a monolayer of non-overlapping cells, (b) homogeneous in shape and surface features, and (c) <10% slide-to-slide variability from a single patient in measured Σ.

Characteristics (a) and (b) were observed using a transmission bright-field microscope while (c) was computed using the HT-PWS system discussed in Section 2.2. The established optimal characteristics were then used as a benchmark to develop and test various standard operating procedures (SOPs). For each protocol, acceptance ratio (ratio of good quality cells to the total cells present within a pre-defined region of a specimen slide) and user variability (same protocol performed by multiple users) were computed. As an example, in the traditional smear deposition protocol discussed in Section 2.5, the user variability was ~30% and the acceptance ratio was ~60% due to the lack of optimal slide/cell quality.

3.2 Liquid based sample collection

The major limitation of the traditional smear deposition protocol (Section 2.5) used for the preliminary results is the high user variability in sample deposition. Figure 4 presents typical cells from specimen slides that were prepared by three different clinical coordinators: A, B and C. Figure 4(a) highlights the poor cell quality due to the rigorous brushing technique followed by coordinator A. In comparison, coordinator C prepared samples with cells that satisfy all the optimal sample conditions above. To understand the diagnostic impact of this user variability in sample preparation, we performed a clinical study on 46 human clinical patients (25 smokers without lung cancer; 21 smokers with lung). These differing methods of preparation had a dramatic effect on the diagnostic performance, with samples collected by coordinator A showing the least significant effect in buccal PWS (ES < 30%) compared to those collected by coordinators B and C (ES > 90%). Consequently, there is a huge need for a sample preparation protocol that is not only stable but also shifts the sample preparation away from the PCP office into a centralized laboratory.

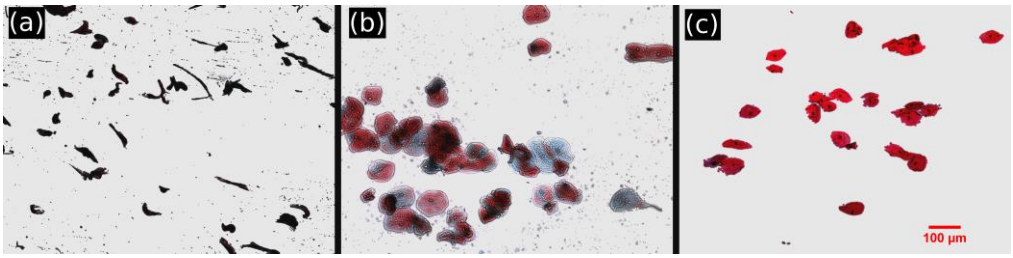

Fig. 4. The smearing deposition is affected by an individual's technique and a majority of the results are not reproducible as observed from intra-coordinator and inter-coordinator comparisons. (a) Clinical coordinator A's smearing technique – the brush was smeared back-and-forth in repetitive motions producing a very poor deposition of cells, (b) Clinical coordinator B's smearing technique – extreme pressure may have been applied on the brush head producing only a few suitable cells, (c) Clinical coordinator C's technique was most suited in producing many suitable cells for PWS analysis

Our group developed a custom liquid-based cell transfer method that reduces the overall variability in sample preparation. With this technique, the cells are first obtained using a cytology brush, then immersed into a vial containing the storage and transport solution. The vial containing the cells in solution is shipped to a centralized facility where slides are prepared using a custom sample deposition system. In order to standardize the liquid based cell transfer method, we identified (i) a suitable storage/transport solution that maximizes the acceptability ratio of the collection; (ii) an optimal sample deposition/transfer method that reduces the user variability of sample preparation and increases the acceptability ratio of the specimen slides; and (iii) an optimal cell transport protocol for shipment of samples from the physician's office to the centralized lab. These protocols were developed and optimized using buccal specimens from 150 human clinical patients and healthy volunteers, and then validated

Biomedical Optics EXPRESS

on 84 human clinical patients by evaluating their performance against the traditional smear deposition method discussed in Section 2.5.

3.2.1 Storage/transport solution

An appropriate storage/transport solution must fix the cells to impede the metabolic process and bacterial growth, minimize mucus and cell debris, while maintaining the cell nanoarchitecture. We tested commercial solutions, such as CytoLyt and Surepath, as well as common fixative/storage solutions such as methanol, ethanol, isopropanol, formaldehyde, glutaraldehyde, etc. on a population of 60 healthy volunteers. Samples were collected in different storage solutions and monitored over time. The storage solution was the only parameter that was varied in these experiments while keeping all other parameters exactly the same. Following sample collection, the samples were deposited (Section 3.2.2), fixed in ethanol, and stained prior to acquisition following the protocol mentioned in Section 2.5(c, f).The effect of the solutions were determined qualitatively (assessing cell suitability) and quantitatively (using Σ). The values of Σ were monitored between the different storage solutions using relative intercellular variability. While the cells in CytoLyt were stable over 10 days, the solution produced excessively overlapped cells, generating a low acceptance ratio (~30%). Similarly, storage solutions such as formaldehyde, glutaraldehyde, etc. made significant alterations to cell structures, resulting in an acceptance ratio < 10%. Low concentrations of ethanol (10% to 45%), in particular 25% ethanol, satisfied our defined 'optimal characteristics'. 25% ethanol kept the samples optimal for up to 10 days without any bacterial contamination (acceptance > 70%) and produced a lower intercellular Σ variability of ~16%. Alternatively, high concentrations of ethanol (> 70%) reduced the quality of cells (acceptance ratio < 10%). While 25% ethanol maintains the shape and structure of the cell, the high concentration of ethanol creates osmotic shock on cells in solution leading to a rapid deterioration of the cell quality.

3.2.2 Optimal sample deposition/transfer method

Once an optimal storage/transport solution was identified, we developed an optimal deposition method to transfer samples onto a specimen slide (clinical samples in preliminary studies were deposited according to Section 2.5(b)). We tested different liquid based cell deposition methods including (a) the commercial Thin Prep kit (Hologic Inc.), (b) a manual deposition of the liquid onto the glass slide using a pipette and (c) a custom developed automated spray deposition method. Our results indicate that the custom spray deposition method using 25% ethanol as a storage solution performs better (acceptance ratio > 70%, user variability < 5%) than the Thin Prep kit, the current gold standard of clinical Pap smear (acceptance ratio ~29%, user variability < 5%). In this enclosed custom-developed spray deposition system, a sample is loaded into an airbrush, attached to a pressurized air-line. An electronic valve is opened via push button switch, causing air to pass a liquid nozzle at high velocity. The shear force of the air passing the liquid produces an aerosol that is propelled towards a glass slide. The fine aerosol produces a thin film of liquid deposited across the slide area. Since the 25% ethanol cell solution dries rapidly after the deposition, the cells form a non-overlapping mono-layer of cells, unlike the overlapping cells observed in the manual cell deposition method using a pipette (acceptance ratio ~48%, user variability ~20%).

The performance of the custom spray deposition method was compared to the traditional smear deposition protocol (Section 2.5) using buccal specimens from 84 clinical patients collected by 3 different clinical coordinators. A typical example of the cells prepared using these two methods is visualized in Fig. 5. As seen, the custom liquid deposition method yields a much higher proption of 'optimal quality cells' (acceptance ratio > 70%) compared to those obtained using the traditional buccal smear deposition method (acceptance ratio < 35%). In addition, the custom spray deposition method had a much lower user variability (< 5%) than the manual smear deposition (~30%).

Biomedical Optics EXPRESS

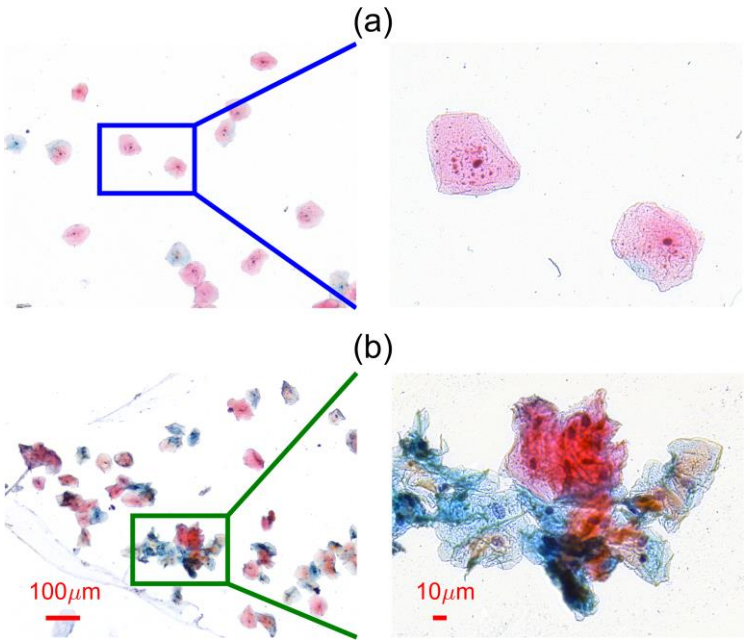

Fig. 5. Representational transmission microscope images of slides prepared following the deposition techniques that were compared for PWS System Lung test SOP optimization. (a) Aerosol deposition at 10x (left) and 40x microscope magnifications (right), (b) Smear deposition at 10x and 40x.

3.2.3 Cell storage and transport protocol

With the advent of liquid based sample collection and transport, temperature requirements must be defined accurately. We tested the samples between 4°C and 40°C for storage over time with samples from healthy volunteer to determine the effect of temperature on a collected sample. A temperature controller was built, based on thermoelectric cooling (Peltier effect), to maintain the various testing temperatures. The collected samples were stored at a single temperature for upto 96 hours or cycled through fluctating temperatures for 24 hour and 48 hour periods to determine the effect of varying temperatures during shipping and transport. Post-storage sample processing remained consistent for all samples: spray deposition (Section 3.2.2), fixation in ethanol and staining prior to acquisition as mentioned in Section 2.5(c, f). For each condition, specimen slide quality and slide-to-slide variability were quantified using Σ. Our results indicated that the cells can be stored between −1°C and 10°C with no increase in Σ (error in $\Sigma < 5\%$) for up to 5 days (acceptance ratio ~70%) from the day of collection. In order to maintain the temperature of the sample between −1°C and 10°C, we worked with a US based scientific products company to develop a cold storage container that would enable us to ship the liquid buccal samples across multiple centers. A temperature indicator is included as part of the shipping container to monitor the maximum sample temperature. To minimize variability, samples were excluded from the clinical study if storage temperature exceeded these tested requirements (occurs in < 2% of the samples).

3.3 Optimal specimen staining protocol

In traditional cytological applications, staining dyes are used to create image contrast due to their absorption properties. Our group has earlier shown that dyes have two effects on optical properties: (a) an absorption at wavelengths where dye absorption occurs and (b) an increase in the overall refractive index outside the absorption range, causing increased scattering [50]. We have shown that staining-induced scattering is ~20 times higher for particles of size ~100

Biomedical Optics EXPRESS

nm relative to the unstained particle of the same size. To develop robust SOPs, it is important to optimize both the cell staining protocol as well as the specimen storage after staining.

In our studies, we utilized a total of 234 buccal specimens from patients with and without lung cancer to optimize the staining for maximized diagnostic performance. Specimen slides were stained using one of the following: Haematoxylin (n = 69), Eosin (n = 60), Aniline Blue (n = 14), and the combined Haematoxylin and Cytostain protocol (n = 91). The results indicated that staining with Haematoxylin and Cytostain yields the best diagnostic performance (>25% increase in Effect size over all other staining protocols). Furthermore, in order to optimize the cell storage after Haematoxylin and Cytostain staining, the value of Σ was evaluated as a function of storage time and temperature, which indicated that the specimen slides can be stored at room temperature (24 ± 3 °C) for up to 10 days with less than a 3% change in Σ.

The results of our protocol development studies highlighted the necessity of maintaining a high level of relative humidity (RH), an environment factor that can contribute to certain artifacts such as highly reflective regions within cells. In essence, when the specimen slides are transitioned from immersion in Ethanol (either during fixation process or at the end of staining procedure) to exposure to air, a low RH leads to rapid evaporation of ethanol particles and the accompanied cellular osmotic stress creates air "pockets" inside the fixed cells. These nanoscale chambers have a refractive index of 1.0 and the light intensity they reflect is orders of magnitudes greater than that from the cell, resulting in a high-reflective appearance under a reflectance-mode microscope. Comparatively, the specimen slides that are fixed and stained at higher RH lack those highly reflective cells. Since PWS is a technique founded on quantification of light-scattering from within the cell, the presence of highly-scattering air chambers wintin a cell is impermissible. Thereby, in all subsequent SOP development processes the RH was maintained above 45%, successfully avoiding the air-chamber artifact.

In summary, our group has developed a robust standardized protocol for buccal PWS nanocytology using 653 specimens from human clinical patients and healthy volunteers (characterization of optimal slide study = 139; liquid cytology study = 280; optimal staining study = 234). The workflow representation of this protocol and the optimal parameter that was developed for each step are shown in Fig. 6. It is important to note that several of these steps, including sample fixation and staining can be accomplished in parallel (as in traditional cytology); therefore, these steps are not rate-limiting for the clinical translation.

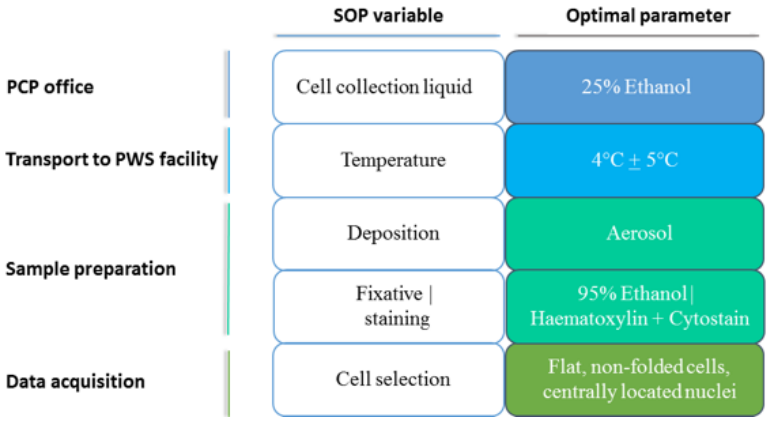

Fig. 6. Structured workflow representation of the final, optimized SOP for the PWS System Lung Test. Standardized parameters were developed and validated on clinical subjects for each stage in the process.

Biomedical Optics EXPRESS

3.4 Validation of the SOP and the HT-PWS instrument

The individual SOP steps and our improved commercial-ready instrument prototype (shown in Fig. 7) were validated in a clinical trial. While the commercial ready system has the same system design architecture as those described in Methods, it was designed and prototyped in a modular manner consisting of: (a) an AOTF-based illumination module with an OEM version of the AOTF, (b) a Microscope module with custom illumination/collection apertures built with off-the-shelf microscope components, and (c) an Embedded PC module with software interfaces to control the HT-PWS system.

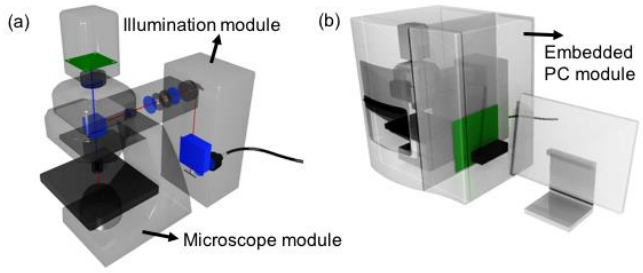

Fig. 7. 3-D model of the commercial-ready HT-PWS prototype that will be implemented in the centralized lab.

The aim of the validation study was to test the clinical performance using the new SOP developed above and compare it with the traditional smear deposition protocol used in previous sets of clinical data. This clinical study was conducted on 37 patients, including 11 cancer-free smokers and 26 lung cancer patients.

Each step of the process was controlled according to developed procedure requirements. Preassembled collection kits were sent to clinical sites to ensure compliance with shipping conditions. Samples were collected from one local collection center (Northshore Health System) and from our collaborators in Boston. The collection kits consisted of a pre-filled collection vial, blank slide and fixation vial for smear collection, gel packs for temperature control, and appropriate labelling. Clinical coordinators were trained on-site on collection, packaging, and shipping protocols. Samples were collected using a cytology brush and transferred to the provided vial with the appropriate transport solution. After collection, samples were packaged in the kits and shipped to the central processing laboratory within 24h. Upon receipt, samples were logged and stored at 4C. The liquid samples were deposited onto glass slides using the custom spray deposition system (section 3.2.2) and fixed in ethanol. Slides were stained using Haematoxylin and Cytostain (rapid Papanicolaou staining) before acquiring PWS data. This data was analyzed and evaluated for diagnostic performance of Σ.

We note that Haematoxylin and Cytostain staining (similar to Papanicolaou technique it approximates) produces two predominant colors in cells: red and blue. This differential polychromatic staining is conventionally used for Pap smears to distinguish mature, superficial squamous cells (which stain red) from metabolically active parabasal or intermediate cells (appear blue) in cervical cancer screening procedures [51].

We have found that when all cells, regardless of their color, are used for the calculation of Σ (as per analysis performed in our preliminary studies), there is a strong differentiation between the smoking controls and patients harboring lung cancer (ES = 96%, p = 0.0001), which is comparable to the difference observed in our previous works [52]. Moreover, upon the implementation of the standardized SOPs, we observed a dramatic decrease in both intra-

Biomedical Optics EXPRESS

and inter-patient variability of Σ compared to our preliminary studies: intra-patient variability reduced from >30% to 8%, and inter-patient variability–from >40% to <8%.

Moreover, detailed data analysis showed that on average intermediate blue cells have a lower Σ compared to red cells, independent of patient diagnosis. Furthermore, when either the intermediate blue- or superficial red-stained cells were used for diagnostic comparison, the differentiation between the two diagnostic groups was also statistically significant ($p < 0.05$). Since the average value of Σ for all blue cells measured from a patient's slide were not correlated to the average value of Σ from red cells (correlation coefficient <0.74 for both smoking controls and lung cancer patients), we used the Σ of intermediate blue cells and superficial red cells as two independent parameters.

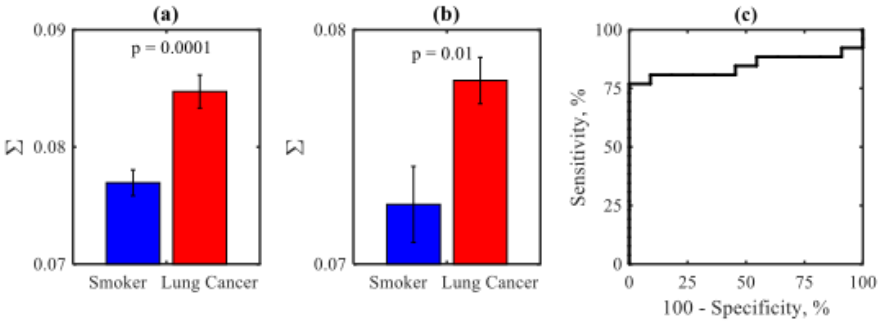

Fig. 8. Results of the validation clinical study (n = 37). Bar plots display the observed statistically significant difference between mean Σ of (a) red cells and (b) blue cells obtained from the smoker control population (n = 11 subjects) and the lung cancer population (n = 26) . (c) ROC curve of the diagnostic performance of Σ based on the two parameter model (AUC = 0.85, Se = 81%, Sp = 91%).

Figure 7 displays the diagnostic results of this two-marker analysis of the validation study data performed following the optimized SOP with the use of the commercial-grade HT-PWS system. The first two plots represent the statistically significant difference in Σ measured from the superficial red (Fig. 8(a)) and intermediate blue (Fig. 8(b)) cells separately, and the third panel shows ROC curve with excellent diagnostic differentiation between the populations with an area under the curve (AUC) of 0.87, sensitivity of 81% and specificity of 91% (Fig. 8(c)). Here, a linear regression model was used to combine the two predictors (Σ of superficial and intermediate cells) yielding a single classifier score optimizing the diagnostics performance, following which the ROC curve was calculated for that combined score. Both the linear regression model parameters and the optimal threshold value were trained and applied to this single set of data.

The results validate the ability of the optimized SOP parameters and the improved PWS instrument to consistently produce samples of very high quality and detect the nanoscale differences with an excellent accuracy. While the protocol and instrumentation validation study only involved 37 patients, compared to the 653 patient samples of the SOP development process, the results provide strong proof that the developed robust-yet-simple SOP parameters are suitable for future multi-center clinical trials and subsequent regulatory approval. Moreover, the SOP studies discussed above also involved multiple case-control diagnostic studies (e.g, optimal cell characteristic, optimal sample processing etc) to confirm that a specific protocol is suitable for translation into a primary care physician's office. It is important to note that the current study was not intended to investigate the fundamental working mechanism of the protocols (e.g, working mechanisms of individual stains, storage/transport solutions etc.). While understanding these mechanisms are of academic interest and may help to further improve the protocols in the future, it is outside the scope of the current study, ultimately intended to find robust protocols for clinical translation.

Biomedical Optics EXPRESS

4. Conclusions and future directions

In conclusion, we have developed and validated a simple, robust and easy to implement standard operating procedures for buccal PWS nanocytology as well as a commercial-ready PWS instrument. We have validated our instrument and the standardized protocol in a clinical study involving 37 human subjects. The improved standardized procedures accomplished a reduction in user variability of prepared slide quality and inter-patient/intra-patient variability in addition to a diagnostic performance consistent with previously reported preliminary results. These studies show a strong proof that in the long term, buccal PWS nanocytology can become a frontline risk stratification tool for personalizing lung cancer screening. Applications of this test can range from an annual exam performed by primary care physicians to investigations by pulmonologists and other specialists. If the buccal PWS test is positive, the patients may be offered more expensive/invasive tests such as LDCT.

With a quality systems and procedures (QSPs) already in place, our next step is to employ the developed SOPs and instrument to perform a multi-center blinded validation trial. We strongly believe that with continued successful trials, buccal PWS nanocytology based risk stratification may one day revolutionize lung cancer screening, leading to a > 90% reduction in lung cancer deaths, similar to the impact the PAP smear on cervical cancer mortality. Moreover, based on our analysis of the National Lung Cancer Screening Trial (NLST) data, it is expected that the buccal PWS based risk stratification test followed by LDCT will dramatically decrease cancer over-diagnosis by more than 85% and will reduce cancer screening costs by over 60%.

Funding

The results presented here are based upon the work supported by National Science Foundation Small Business Innovation Research program under Grant IIP-1214989, Grant from LUNGevity Foundation and the National Institutes of Health Small Business Innovation Research Program under Grant 1R44CA168185, the National Institutes of Health under Grants: R01EB016983, R01CA155284. Drs. Subramanian, Backman and Roy are cofounders and/or shareholders in NanoCytomics LLC. All aspects of this study were done under the supervision of the Conflict of Interest Committee at Northwestern University.

Acknowledgments

The authors would like to thank John Chandler for the help with the PWS instrumentation; Di Zhang for the help with numerical model of PWS nanocytology; John Hart and Mirela Wohlford for the help in guiding us through the steps involved in clinical translation.